Journal of Physics: Photonics

OPEN ACCESS

RECEIVED
20 October 2021

REVISED
14 December 2021

ACCEPTED FOR PUBLICATION
5 January 2022

PUBLISHED
24 January 2022

PAPER

High-energy bow tie multi-pass cells for nonlinear spectral broadening applications

Christoph M Heyl[1,2,3,*], **Marcus Seidel**[1], **Esmerando Escoto**[1], **Arthur Schönberg**[1], **Stefanos Carlström**[4,5], **Gunnar Arisholm**[6], **Tino Lang**[1] and **Ingmar Hartl**[1]

[1] Deutsches Elektronen-Synchrotron DESY, Notkestraße 85, 22607 Hamburg, Germany
[2] Helmholtz-Institute Jena, Fröbelstieg 3, 07743 Jena, Germany
[3] GSI Helmholtzzentrum für Schwerionenforschung GmbH, Planckstraße 1, Darmstadt, 64291, Germany
[4] Department of Physics, Lund University, Box 118, SE-221 10 Lund, Sweden
[5] Max-Born-Institut, Max-Born-Straße 2A, 12489 Berlin, Germany
[6] FFI (Norwegian Defence Research Establishment), P. O. Box 25, NO-2027 Kjeller, Norway
[*] Author to whom any correspondence should be addressed.

E-mail: christoph.heyl@hi-jena.gsi.de

Keywords: post-compression, spectral broadening, multi-pass cell, nonlinear optics, high energy laser

Abstract

Multi-pass cells (MPCs) have emerged as very attractive tools for spectral broadening and post-compression applications. We discuss pulse energy limitations of standard MPCs considering basic geometrical scaling principles and introduce a novel energy scaling method using a MPC arranged in a bow tie geometry. Employing nonlinear pulse propagation simulations, we numerically demonstrate the compression of 125 mJ, 1 ps pulses to 50 fs using a compact 2 m long setup and outline routes to extend our approach into the Joule-regime.

1. Introduction

Ultrashort laser pulses play a crucial role in many fields ranging from time- and frequency domain spectroscopy and strong-field physics to surgery and welding [1]. The amplification of ultrashort pulses set constraints on their duration imposed by bandwidth limitations. The most common ultrafast high-power laser platforms are nowadays titanium:sapphire (Ti:Sa) and ytterbium (Yb)-based systems, providing amplified pulses with durations ranging from a few tens of fs (Ti:Sa) to hundreds of fs (Yb). Two different methods are commonly employed to overcome these pulse width limits: parametric amplification [2] and post-compression [3]. The latter method relies on nonlinear spectral broadening and either simultaneous or subsequent temporal compression. Various spectral broadening methods have been commonly used including nonlinear propagation within a single [4] or multiple plates [5], within solid-core [6] and photonic crystal fibers [7], hollow-core capillaries (HCCs) [8], filaments [9] or slab waveguides [10]. Recently, a new method based on nonlinear spectral broadening within multi-pass cells (MPC) was introduced [11, 12]. The method offers high transmission [13, 14], high-power handling [14, 15], excellent beam quality [13, 16] and large compression ratios [16, 17] while being easily adaptable to a large variety of laser pulse parameters including durations ranging currently from 10 ps [18] to few-cycles [17, 19, 20] as well as pulse energies ranging from a few μJ [21] to more than 100 mJ [22].

A key challenge is the adaption of high-performance post-compression methods to high pulse energies. In particular, advancing post-compression methods into the Joule-class pulse energy regime could enable the application to strong-field physics with the potential to overcome peak power limitations of chirped-pulse amplification [23]. While approaches like HCC, MPC or filament-based methods can in principle be scaled to very high pulse energies [24], the required setup-sizes become impractically large. Alternative approaches have employed thin films as nonlinear media to spectrally broaden Joule-class pulses [23]. These methods suffer, however, from reduced beam quality compared to HCC and MPC-based methods and only small compression factors could be reached so far. Spatial and/or temporal pulse multiplexing methods have also

been suggested for pulse energy scaling [25, 26], increasing, however, system complexity especially at large multiplexing factors.

Here we outline basic geometrical energy scaling principles for MPCs and introduce a novel pulse energy scaling method. Our approach enables compact setups while maintaining advantageous properties of standard MPCs such as high throughput, high compression ratios and excellent beam quality. Using nonlinear pulse propagation simulations, we demonstrate compression of 125 mJ, 1 ps pulses at 1030 nm to 50 fs using a compact setup of 2 m length while maintaining a reasonable fluence at all mirrors. Moreover, via analytical energy scaling relations, we present routes to scale our approach to Joule-class pulses and present a first numerically tested example configuration at 1 J.

2. Pulse energy limits of standard MPCs

We start by considering a standard Herriott-type MPC [27] with two identical concave mirrors with radius of curvature R placed at a distance L as discussed e.g. in [28]. A reentrant beam pattern with N round trips through the MPC can be reached by obeying the simple relation [27, 29]:

$$C = \frac{L}{R} = 1 - \cos\left(\frac{\pi k}{N}\right), \tag{1}$$

with $k = 1, \ldots, N-1$ denoting a variable integer which is related to the angular advance of consecutive beam spots on one MPC mirror $\xi = 2\pi k/N$ [27]. In order to obtain a q-preserving MPC ensuring similar nonlinear pulse propagation characteristics for each round trip, the input beam needs to be mode-matched to the eigenmode of the MPC, which is identical to the mode of a corresponding cavity. Considering basic properties of a two-mirror cavity, the fundamental Gaussian eigenmode can be derived by solving the identity condition for the Gaussian beam parameter $q = (M_1 q + M_2)/(M_3 q + M_4)$ with M_i denoting the elements of the $ABCD$ matrix for a single round trip through the cavity. The corresponding focal spot radius w_0 of a linearly mode-matched beam (neglecting the impact of Kerr lensing on the MPC eigenmode) can be written as:

$$w_0^2 = \frac{R\lambda}{2\pi}\sqrt{C(2-C)} = \frac{R\lambda}{2\pi}\sin(\pi k/N) \overset{k/N\to 1}{\approx} \frac{R\lambda}{2N}, \tag{2}$$

expressed as a function of the integer variables k and N for a reentrant beam pattern or more generally as a function of the configuration parameter $C = L/R$, which can also be used for non-reentrant MPCs. Mode matching is possible for stable resonators, i.e. for $0 < C < 2$. Equation (2) also provides an approximate solution for the typical operation condition close to the outer stability edge at $k = N-1$ in the limit $N \to \infty$. Here and in the following, we use the simplified notation $k/N \to 1$ to express this limit. In this limit, the focal spot size w_0 is minimized and the beam spot size at the mirrors w_m reaches a maximum. Using simple Gaussian beam equations w_m can be derived from equation (2) yielding:

$$w_{\mathrm{m}}^2 = \frac{R\lambda}{\pi}\sqrt{\frac{C}{2-C}} = \frac{R\lambda}{\pi}\tan(\pi k/2N) \overset{k/N\to 1}{\approx} \frac{2R\lambda N}{\pi^2} \approx \frac{L\lambda N}{\pi^2}. \tag{3}$$

In order to spectrally broaden an input pulse, a nonlinear medium such as a gas or a glass plate can be inserted into the MPC. Considering self-phase modulation-based pulse propagation governed by the intensity-dependent refractive index change $\Delta n = n_2 I$, the pulse energy E can be increased while maintaining key broadening characteristics by decreasing the nonlinearity. For gas-filled MPCs, the gas pressure p provides a simple way to tune the nonlinear refractive index $n_2 \propto p$. For constant setup size, energy up-scaling is however limited by the laser-induced damage threshold (LIDT) F_{th} of the MPC mirrors and by the focus peak intensity I_0 setting a limit via ionization at a threshold intensity I_{th}. Peak fluence at the MPC mirrors and peak focus intensity of a linearly mode-matched beam can be calculated as:

$$F_{\mathrm{m}} = \frac{2E}{R\lambda}\sqrt{2/C-1} = \frac{2E}{R\lambda}\frac{1}{\tan(\pi k/2N)} \overset{k/N\to 1}{\approx} \frac{\pi E}{R\lambda N}, \tag{4}$$

$$I_0 = \frac{4P}{R\lambda}\frac{1}{\sqrt{C(2-C)}} = \frac{4P}{R\lambda}\frac{1}{\sin(\pi k/N)} \overset{k/N\to 1}{\approx} \frac{4PN}{\pi R\lambda}. \tag{5}$$

The maximum laser pulse energy thus reads as:

$$E_{\max} < \min\left[\frac{F_{\mathrm{th}} R\lambda}{2\sqrt{2/C-1}},\ I_{\mathrm{th}} R\lambda\tau\frac{1}{4}\sqrt{C(2-C)}\right]. \tag{6}$$

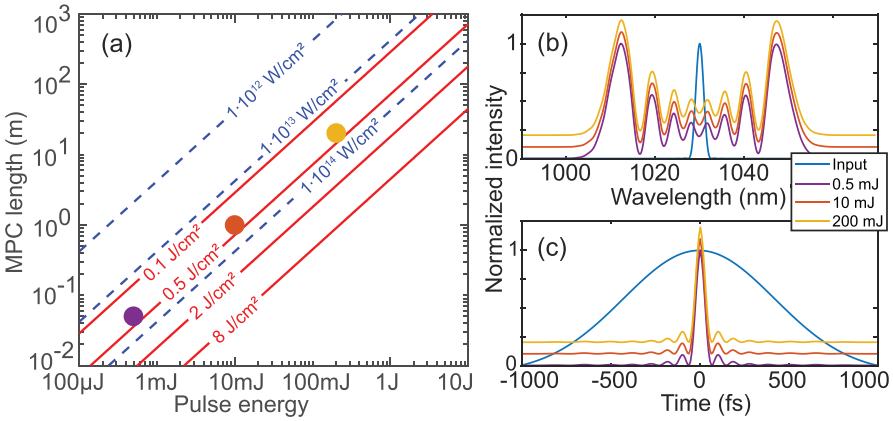

Figure 1. (a) MPC setup length as a function of pulse energy considering limitations arising due to the mirror LIDT and focus intensity for a standard Herriott-type MPC with reentrant beam-pattern and $k/N = 14/15$. The colored markers indicate example configurations at 5, 10 and 200 mJ using 1 ps input pulses at 1030 nm. The corresponding broadened spectra and compressed pulses (Fourier transform limit) simulated using three-dimensional nonlinear pulse propagation are shown in (b) and (c), respectively. The offset in (b) and (c) is introduced for clarity.

Taking the example of an MPC with $R = 1$ m operated close to the stability edge with $k/N = 14/15$, $\lambda = 1030$ nm and pulse width $\tau = 1$ ps, and considering a mirror damage threshold of $F_{\mathrm{th}} = 500$ mJ cm^{-2}, we obtain an energy limit of 24.5 mJ and a corresponding peak focus intensity of $4.6 \cdot 10^{13}$ W cm^{-2} at an MPC length of $L = R \cdot C = 1.978$ m.

In order to increase the pulse energy beyond this limit, the inequalities in equation (6) indicates multiple tuning parameters: C (tunable via k/N), λ and R. For $k/N \to 1$, F_{m} decreases but I_0 increases. While the fluence-based pulse energy limit can thus be increased, ionization effects in the focus limit the maximum pulse energy for gas-filled MPCs. In addition, the MPC imaging properties at the stability edge $k/N = 1$ prevent homogenization of the spatial beam profile during the broadening process. Earlier works reporting the operation of MPCs at the stability edge (equivalent to a $4f$ imaging geometry) yielded reduced spatial beam quality characteristics at rather low compression ratio [30]. Both limits defining E_{max} scale linearly with λ, thus allowing larger pulse energies for longer wavelengths if F_{m} can be kept constant.

The practically most effective pulse energy tuning option for a standard MPC is provided by the setup size, represented by R in equation (6), showing a straightforward linear scaling relation for the maximum pulse energy. Scaling the pulse energy linearly with setup length enables not only a constant intensity at the mirrors and in the focus, it further ensures fully scale-invariant spectral broadening characteristics provided that the pressure is reduced linearly with increasing pulse energy. The fundamental principle behind this energy scaling method is outlined in a more general context in [24] and can be motivated by basic scaling properties of the nonlinear wave equation, which can be used to describe the nonlinear pulse propagation process inside the MPC. In paraxial approximation and considering a Kerr-induced nonlinear polarization $\hat{\mathcal{P}}_{\mathrm{NL}}$, this equation can be written for the field envelope $\hat{\mathcal{E}}$ as [24]:

$$\left[\frac{\partial}{\partial z} - \frac{i\lambda}{4\pi n}\Delta_\perp - i\frac{2\pi}{\lambda}(n-1)\right]\hat{\mathcal{E}} = \frac{i\pi}{n\lambda\epsilon_0}\hat{\mathcal{P}}_{\mathrm{NL}}(\rho), \tag{7}$$

where n, λ, ϵ_0 and ω, ρ denote refractive index, vacuum wavelength and permittivity as well as angular frequency and gas density, respectively. $\Delta_\perp$ denotes the transverse radial Laplace operator. Taking into account linear pressure dependencies $(n-1) \propto \rho, \hat{\mathcal{P}}_{\mathrm{NL}} \propto \rho$ and neglecting the weak pressure dependence of n in the denominator of the diffraction and the nonlinear terms, it can be shown that any solution of equation (7), $\hat{\mathcal{E}}(r\eta, z\eta^2, \rho/\eta^2)$ is fully scale-invariant if longitudinal coordinates z, radial coordinates r and the gas density are scaled appropriately with pulse energy $E \propto \eta^2$, using a general scaling parameter η.

We thus obtain fully scale-invariant spectral broadening characteristics which do not depend on the laser pulse energy if setup size and gas density are scaled appropriately with pulse energy [24]:

$$\begin{aligned} R, L &\propto E \\ \rho &\propto 1/E. \end{aligned} \tag{8}$$

Most importantly, there is no fundamental upper limit for the pulse energy via geometrical setup size scaling. In practice the limit is simply the setup size itself, as illustrated in figure 1. While setup lengths in the order of 1 m can be employed to compress 1 ps pulses with about 10 mJ, the setup length would increase to

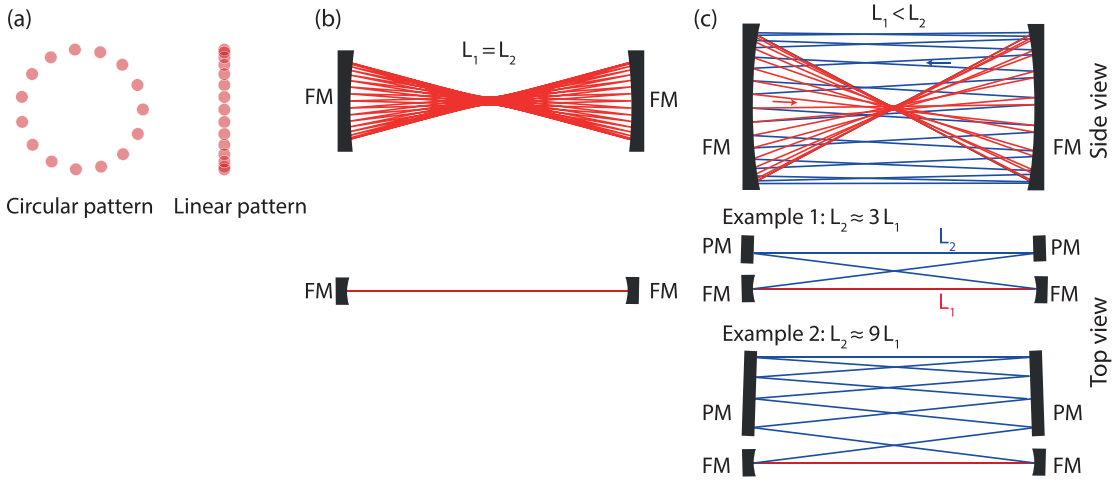

Figure 2. (a) Commonly used circular beam patterns at the focusing mirrors together with a linear beam pattern as used for the BT-MPC. (b), (c) Illustration of multi-pass beam pattern geometries for a standard MPC (b) and a BT-MPC (c). In (b), (c) the beam path projections onto the vertical plane (top panels) and the corresponding projections onto the horizontal plane (middle and bottom panels) are shown, visualizing example configurations with three and nine times folded paths for the BT-MPC (c). Note that the top panel beam path is simplified for clarity: the beams along L_2 (blue) folded via plane mirrors (PMs), are depicted as straight paths between the focusing mirrors (FMs) instead of folded paths.

20 m for 200 mJ, making further energy scaling impractical. Conversely, energy down-scaling is possible via a geometrical setup size reduction as indicated in figures 1(b) and (c) for 0.5 mJ, spectrally broadened in a 5 cm setup. Similar scaling principles can also be applied to bulk-based MPCs. As the density of the nonlinear medium cannot easily be changed, deviations from perfect scale-invariance can however be expected.

3. Bow tie multi-pass cells

We now introduce a pulse energy scaling route, which circumvents the above discussed setup size limitations. We employ known design principles for optical resonators, where large mode sizes can be achieved in a folded cavity design. Applying those principles and placing all folding mirrors in sections of large beam sizes, allows us to construct MPCs of compact size which support high pulse energies.

One of the most simple generalizations of a two-mirror resonator is a four-mirror resonator, often arranged in a so-called bow tie configuration. We here consider a corresponding bow tie MPC (BT-MPC) using two identical concave mirrors and two (or more) plane mirrors. This way, an MPC can be constructed for which the optical path L_1 from mirror 1 to mirror 2 has a different length compared to the returning path $L_2 \neq L_1$, as illustrated in figure 2. A typical bow tie configuration would be reached when L_2 is folded by two plane mirrors. Generally, a BT-MPC can be arranged in different geometrical configurations. Figure 2 displays an example configuration utilizing a linear multipass pattern at the focusing mirrors in contrast to standard Herriot-type MPCs, which are usually arranged with circular pattern. As discussed by Herriott, elliptical or even linear patterns are easily possible depending on the input beam conditions [27].

Similar to equation (1), a general equation describing the solutions for a reentrant beam pattern in a BT-MPC with two identical concave mirrors of radii R and two or more planar folding mirrors can be derived. A reentrant MPC can be obtained if $(\tilde{M}^*)^N = \tilde{I}$, where the $ABCD$ matrix $\tilde{M}^*$ describes a single round trip through the MPC and $\tilde{I}$ denotes the unity matrix with its elements $A_N = D_N = 1$. An equation describing the reentrant MPC can be found via the Gouy phase ξ accumulated during N round trips through the MPC [31]:

$$\xi_N = \mathrm{sgn}(B_N)\cos^{-1}\left(\frac{A_N + D_N}{2}\right). \tag{9}$$

With $(\tilde{M}^*)^N = \tilde{I}$, equation (9) predicts the condition $\xi_N = 2\pi k$ with k denoting a variable integer. Assuming an optimized configuration where the beam acquires the same Gouy phase per pass through the MPC, we obtain for a single round trip:

$$\xi_1 = 2\pi k/N, \tag{10}$$

By solving equation (9) for $N = 1$ taking into account equation (10) and a suitable (M^*) describing the BT-MPC we obtain:

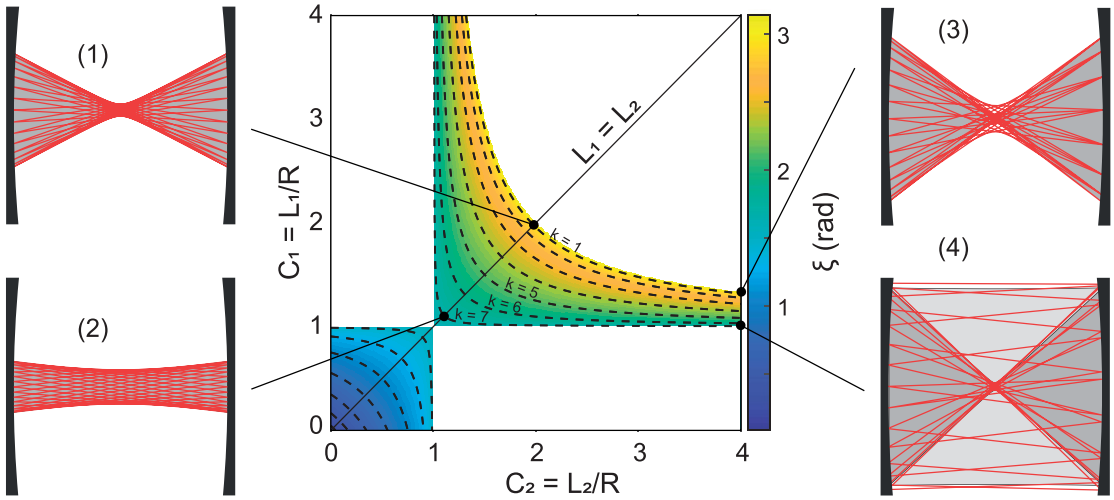

Figure 3. Stability diagram for the bow tie MPC showing the Gouy phase accumulated per pass through the MPC. The dashed black lines indicate reentrant input-to-output 1:1 imaging conditions for an example configuration with N = 15. The standard MPC parameter space with $L_1 = L_2$ is indicated with a black diagonal line. Beam pattern geometries (red) and corresponding cavity modes (gray areas, scaled in diameter to match the pattern size) shown for four important example configurations for constant L_1 and variable R.

$$C_1 + C_2 - C_1\,C_2 = \sin^2(\pi k/N) \quad \text{with } k = \begin{cases} 1,2,\ldots,N/2-1, & \text{if } N \text{ is even} \\ 1,2,\ldots,(N-1)/2, & \text{if } N \text{ is odd} \end{cases}, \tag{11}$$

with $C_{1,2} = L_{1,2}/R$ defined analogously to equation (1). The solutions of equation (11) $C_1 = C_1(C_2, k/N)$ are shown in figure 3 (dashed black lines) using the example of $N = 15$ for $k = 1,2,\ldots,7$. We consider in the following the parameter range $C_{1,2} > 1$ with a tightly focused short beam path along L_1 and a weakly focused beam along L_2, i.e. $L_2 > L_1$. It can be shown that equation (11) describes lines with constant stability parameter G. Here, G is defined analogously to resonator optics as $G = |(A+D)/2| = \cos^2(\pi k/N)$ with A and D denoting elements of an $ABCD$ matrix describing a single round trip through the MPC. Figure 3 also displays the accumulated Gouy phase ξ after a single pass through the MPC. The white areas mark regions outside the stability range ($G > 1$). Equation (11) convergences towards equation (1) for $L_1 = L_2$, representing the standard two-mirror Herriott cell. At the stability edge for $k/N = 1$, the BT-MPC converges towards a $4f$ imaging configuration as explored in [30].

We now calculate basic properties of the BT-MPC assuming linear mode matching, i.e. neglecting Kerr lensing effects in the MPC. This simplification enables the derivation of simple analytical equations. Depending on the operation regime, Kerr lensing effects need to be taken into account to allow an accurate estimate of the MPC parameters [32, 33], as shown in section 4. The focal spot radii $w_{0_{1,2}}$ of a beam linearly mode-matched to the fundamental Gaussian eigenmode of a BT-MPC can be calculated as:

$$w_{0_1}^2 = \frac{R\lambda}{4\pi}\frac{|\sin(2\pi k/N)|}{C_2 - 1} \underset{N\text{ odd}}{\overset{k/N\to 1/2}{\approx}} \frac{R\lambda}{4N(C_2-1)}, \tag{12}$$

$$w_{0_2}^2 = \frac{R\lambda}{2\pi}(C_2 - 1)|\tan(\pi k/N)| \underset{N\text{ odd}}{\overset{k/N\to 1/2}{\approx}} \frac{R\lambda N}{\pi^2}(C_2-1), \tag{13}$$

where $w_{0_{1,2}}$ denote the two foci with $w_{0_2} > w_{0_1}$ for $L_2 > L_1$. The above equations display approximated solutions for $k = (N-1)/2$ in the limit $N \to \infty$ considering an odd integer N. Again, we use a simplified notation to express this limit: $k/N \to 1/2$ with N odd. The limit denotes the operation condition for which the spot size ratio w_{0_2}/w_{0_1} and the beam sizes at all mirrors are maximized. Note that the mirror spot size for a standard MPC is maximized for $k/N \to 1$ instead. For large w_{0_2}, the beam along L_2 appears approximately collimated, i.e. $w_m \approx w_{0_2}$ with increasing beam diameter as L_2 increases. A collimated beam along L_2 brings along an important advantage of the BT-MPC: the beam path can be folded without increasing the maximum mirror fluence, providing great opportunities for the construction of compact MPC systems as the system length is only determined by $L_1 \approx R$. Assuming linear mode-matching, the fluence at the focusing mirrors can be estimated as:

$$F_m^* = \frac{4E}{R\lambda(C_2-1)\tan(\pi k/N)} \underset{N\text{ odd}}{\overset{k/N\to 1/2}{\approx}} \frac{2\pi E}{R\lambda N(C_2-1)}. \tag{14}$$

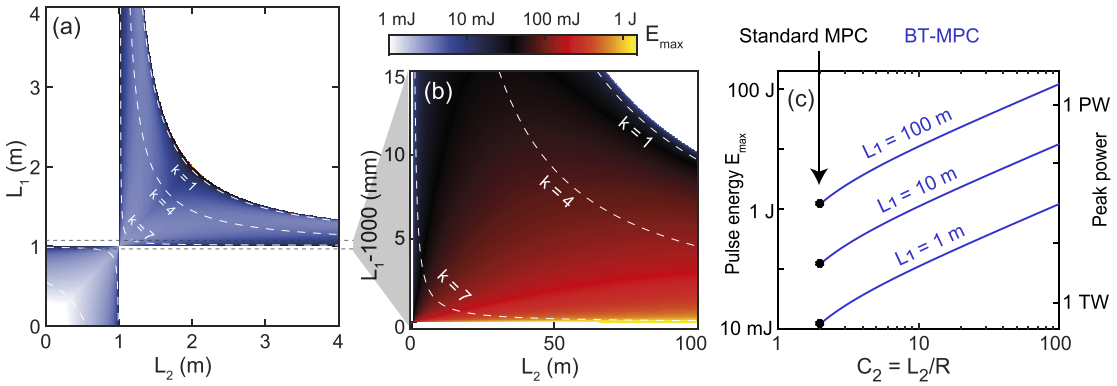

Figure 4. (a), (b) Fluence-limited laser pulse energy for a BT-MPC displayed as a function of $L_{1,2}$ considering $R = 1$ m with (b) showing a rescaled section of (a). (c) Fluence-limited pulse energy as a function of C_2 for different setup lengths L_1. In (c), we also display the corresponding peak power assuming compression to 50 fs. The black circles indicate the fluence-limited pule energy of a corresponding standard MPC. Parameters used: $N = 15$, $k = 7$ (c), $F_{\mathrm{th}} = 0.5\,\mathrm{J\,cm^{-2}}$.

The corresponding maximum focus peak intensity occurring at the focus along L_1 reads as:

$$I_{0_1}^{*} = \frac{8P(C_2-1)}{R\lambda|\sin(2\pi k/N)|} \underset{N\ \mathrm{odd}}{\overset{k/N\to 1/2}{\approx}} \frac{8PN(C_2-1)}{\pi R\lambda}. \tag{15}$$

While the beam spot sizes at the mirror surfaces increases with L_2 causing a decreasing fluence, the focus peak intensity at the tighter focus intersected by L_1 increases. Ionization at the tight focus of the BT-MPC can be avoided by operation inside a vacuum chamber at a low residual gas pressure. For spectral broadening one or multiple glass plates can be placed within a section of the MPC with large beam diameter. Thus, the fluence on the mirrors is the only pulse energy limit:

$$E_{\mathrm{max}}^{*} \leqslant F_{\mathrm{th}}R\lambda(C_2-1)\frac{|\tan(\pi k/N)|}{4} \underset{N\ \mathrm{odd}}{\overset{k/N\to 1/2}{\approx}} \frac{F_{\mathrm{th}}R\lambda N}{2\pi}(C_2-1). \tag{16}$$

With increasing L_2, E_{max}^{*} increases reaching values above 1 J for $L_2 = 100$ m and $L_1 \approx 1$ m as illustrated in figure 4. In figure 4(c), the fluence-limited E_{max}^{*} is displayed as a function of C_2 for different system lengths L_1 together with the corresponding peak power reached assuming for simplicity a Gaussian pulse shape and compression to 50 fs. At large asymmetries L_2/L_1, the collimated beam path along L_2 has to be folded many times in order to keep the system compact. This is possible using today's multi-layer mirror technology supporting pulse durations of <30 fs with losses at the few-parts per million level, thus enabling system transmissions above 90% even for a large number of mirror reflections.

For increasing asymmetry L_2/L_1, the stability range of a BT-MPC decreases, as visible in figure 4. This implies increasing stability demands on the setup, in particular with respect to the distance L_1. Small changes of L_1 can translate into mode-matching issues. Depending on the exact geometry, variations of L_1 from round trip to round trip may occur, in particular if geometries using linear multi-pass patterns, as illustrated in figure 2, are used. In addition, it is advantageous to design the BT-MPC such that all angles of incidence at the focusing mirrors are kept small in order to minimize astigmatism. While these constraints will need to be considered for a experimental setup design, they are not setting a fundamental limit for the proposed scaling approach using BT-MPCs. Possible solutions to circumvent these constraints may include the division of the focusing and/or folding mirrors into multiple small mirrors, providing increased flexibility for beam angle control, enabling e.g. to place all mirrors in a cylindrically symmetric arrangement.

4. Numerical verification of the BT-MPC scheme

In order to test the applicability of BT-MPCs to high peak power spectral broadening, we conducted two-dimensional (2D+1) nonlinear pulse propagation simulations with the SISYFOS code assuming radial symmetry and considering the Kerr effect (Raman and ionization are not included as these effects are not relevant for the parameters considered). Example BT-MPC configurations were tested with a full three-dimensional (3D+1) version of the code, confirming good agreement with the radially symmetric code. The code was previously applied to bulk and MPC broadening simulations [32, 34]. We selected thin silica plates as nonlinear media and consider a MPC placed inside a vacuum chamber to avoid ionization at the focus. The fluence at the Kerr plates as well as the Kerr-lensing effect were minimized by placing the silica

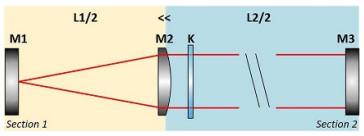

Figure 5. BT-MPC-equivalent resonator used for simulations. It consists of two sections separated by a dispersion-free lens (M2). The plane mirrors M1, M3 are inversion centers of the BT-MPC. Section 1 represents the short arm of the BT-MPC. To save computational costs, an equivalent path with beam inversion was simulated. Pulse propagation in the long arm (section 2), which contains the Kerr-medium (K) was simulated by nonlinear propagation.

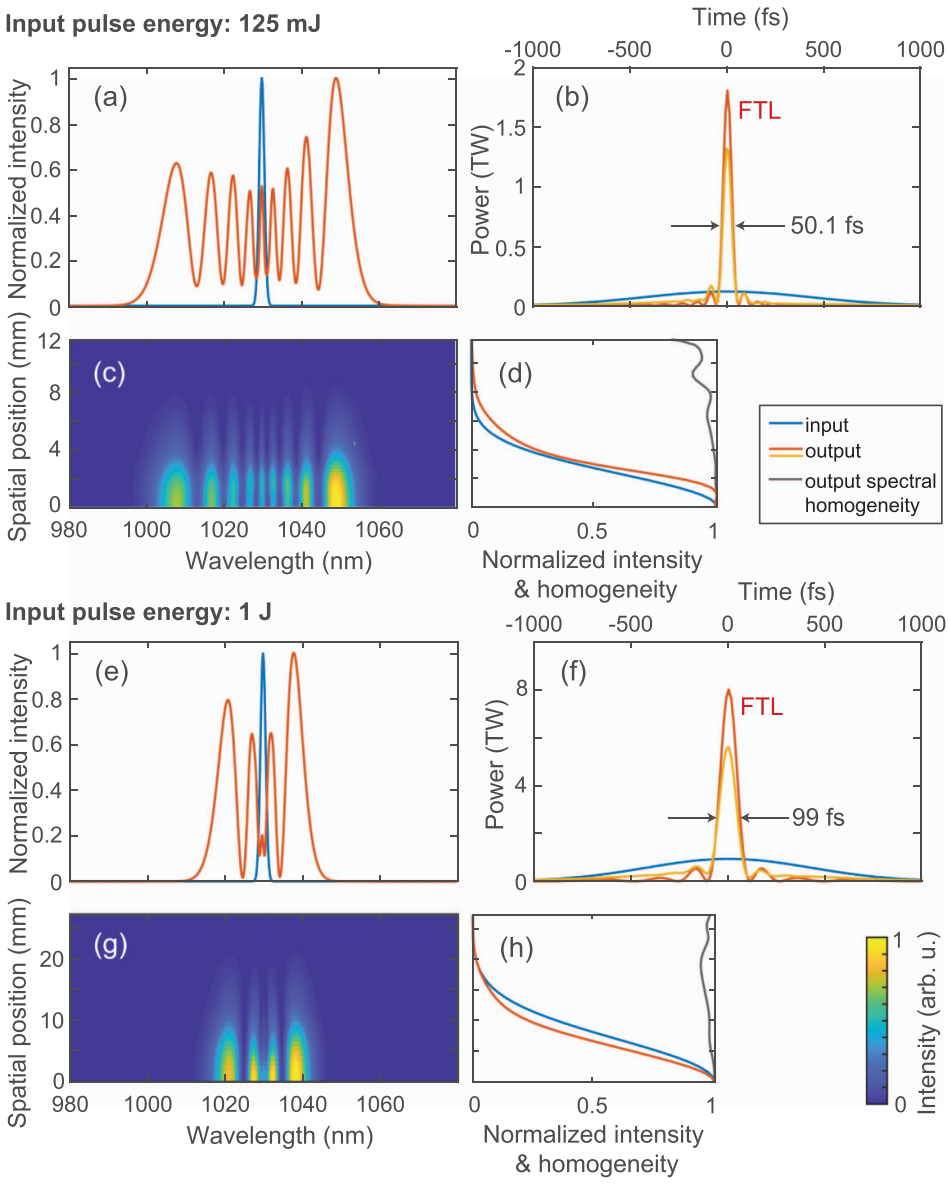

Figure 6. Simulated broadened spectra (red), displayed in (a), (e) and corresponding temporal intensity of the compressed pulses (orange), displayed in (b), (f), spectrally broadened in two different BT-MPCs with pulse energies of 125 mJ (a)–(d) and 1 J (e)–(h). The corresponding input beam spectra and temporal intensities are also shown (blue). The spatially resolved output spectra are displayed in (c), (g) together with the corresponding input (blue) and output (red) spatial beam profiles as well as the spatial homogeneities (gray), shown in (d), (h). The Fourier transform limited (FTL) pulse duration is also depicted (red), displayed in (b), (f).

plates close to the curved mirrors in the long arm of the BT-MPC. For the simulations, a BT-MPC equivalent cavity was considered which is shown in figure 5. Virtual plane mirrors are introduced at the symmetry planes.

First, we simulate spectral broadening of Gaussian pulses with 1 ps duration and 125 mJ energy considering an initially Gaussian spatial beam shape. In the absence of nonlinearity, the BT-MPC consists of

focusing mirrors with a radius of curvature of 2 m and an unfolded arm length of $L_2 = 10$ m. In order to reach a large spot size on the mirrors we consider $k \approx N/2$, i.e. $L_1 = R + \delta$ with $\delta = 2$ mm. The corresponding peak intensity in the long arm was 360 GW cm^{-2} (360 mJ cm^{-2}). To achieve a minimum fluence level at the mirror when Kerr nonlinearity is introduced, we apply nonlinear mode-matching methods [32, 33]. Nonlinear mode-matching can be reached by adjusting the input beam parameters e.g. via adjusting the input spot size at the virtual plane mirror M3. For the BT-MPC geometry considered here, this simple approach is not sufficient to reach a fluence level at the mirrors below damage threshold. Therefore, additional cavity length adjustments are required. Extending the long arm length to $L_2 = 35$ m results in spatially homogeneous broadening and only moderate fluence enhancements compatible with the damage thresholds of the optics. The MPC length lies in the range of demonstrated solid-state laser oscillators with a repetition rate of 8.6 MHz [35]. The implementation of such a BT-MPC therefore appears feasible. Folding of the long arm can lead to a physical length of the cavity of only about 2 m. After 34 round trips in the cavity, a broadening factor of 20 is reached with two 1-mm thick Kerr media placed symmetrically close to the focusing mirrors. A large round trip number is chosen to reduce the B-integral per pass required for the targeted compression factor, as a reduced B-integral simplifies nonlinear mode-matching. The resulting broadened spectrum is shown in figure 6(a). We test the compressibility of the pulses by simulating a dispersive mirror compressor. A flat group delay dispersion (GDD) of -400 fs^2 per bounce is added to the full electric field obtained from the MPC simulation until the peak power was maximized. After 25 bounces a near transform-limited pulse with a duration of 50 fs and a peak power of 1.3 TW is reached (b), assuming an MPC transmission of 87% and a lossless compressor. Figures 6(c) and (d) show spatially resolved spectrum, beam profile and homogeneity parameter parameter (defined as in [21]), indicating excellent spatial output beam quality. The numerically calculated M^2 value of the output beam is $M^2 = 1.15$. Direct calculation of M^2 is very sensitive to numerical noise in the winds of the spatial beam profile, we therefore use a method mimicking a realistic experimental scenario as implemented by commercially available M^2 measurement tools, i.e. considering propagation of the output beam through a focus while applying spatial apertures with a diameter equal to twice the knife edge beam width at a 10/90 intensity fraction.

In a second study, we increase the pulse energy from 125 mJ to 1 J. In order to keep the fluence on the mirrors comparable to the previous example, a long arm length of $L_2 = 75$ m is required in the linear propagation regime if δ is reduced to 0.1 mm. Nonlinear mode-matching for a 1 mm thick substrate per half-cavity results in a long arm length of 276 m, i.e. a relatively large extension comparable to the 125 mJ case. While this optical path length reaches the limits of earlier demonstrated oscillator lengths [35], it should be noted that an MPC has reduced stability requirements compared to oscillators as no longitudinal modes are formed. Figure 6(e) shows the spectral broadening of the 1 ps pulses after 14 round trips. Compression is simulated taking into account dispersive mirrors with a GDD of -1000 fs^2. A pulse duration of 99 fs (96 fs Fourier transform limit) was achieved by adding a total GDD of $-15\,000$ fs^2. The resulting peak power is 5.6 TW under the assumption of 94.5% total transmission (f). Again, an excellent spatial beam quality is achieved at the output (g,h) corresponding to $M^2 = 1.08$.

5. Conclusion

We have discussed general pulse energy scaling principles and limitations for MPCs employed for spectral broadening applications and introduced a new MPC type. The new MPC design enables large beam spot sizes at all mirror surfaces and thus operation at high pulse energies while keeping the setup size compact. In contrast to other guided-wave spectral broadening approaches, our method supports very high spatial beam quality despite the large pulse energies and broadening factors. Our analytical analysis shows, that highly efficient MPC-based pulse-post compression at large compression ratios can be extended to 100 mJ pulse energies and beyond using a table-top setup. More generally, our results extend the concept of multi-pass spectral broadening to non-standard MPCs demonstrating a viable route to greatly expand the parameter space of multi-pass post-compression.

Data availability statement

The data that support the findings of this study are available upon reasonable request from the authors.

Acknowledgment

We acknowledge Helmholtz-Institute Jena (Jena, Germany) and DESY (Hamburg, Germany), members of the Helmholtz Association HGF, for support and the provision of experimental facilities.

ORCID iDs

Christoph M Heyl https://orcid.org/0000-0003-2133-5224
Stefanos Carlström https://orcid.org/0000-0002-1230-4496
Gunnar Arisholm https://orcid.org/0000-0002-8058-7969

References

[1] Mourou G 2019 Nobel lecture: extreme light physics and application *Rev. Mod. Phys.* **91** 030501
[2] Fattahi H *et al* 2014 Third-generation femtosecond technology *Optica* **1** 45–63
[3] Nagy T, Simon P and Veisz L 2020 High-energy few-cycle pulses: post-compression techniques *Adv. Phys.* X **6** 1845795
[4] Rolland C and Corkum P B 1988 Compression of high-power optical pulses *J. Opt. Soc. Am.* B **5** 641
[5] Chih-Hsuan L, Tsou Y-J, Chen H-Y, Chen B-H, Cheng Y-C, Yang S-D, Chen M-C, Hsu C-C and Kung A H 2014 Generation of intense supercontinuum in condensed media *Optica* **1** 400
[6] Stolen R H and Lin C 1978 Self-phase-modulation in silica optical fibers *Phys. Rev.* A **17** 1448–53
[7] Knight J C, Birks T A, Russell P S J and Atkin D M 1996 All-silica single-mode optical fiber with photonic crystal cladding *Opt. Lett.* **21** 1547
[8] Nisoli M, Silvestri S D and Svelto O 1996 Generation of high energy 10 fs pulses by a new pulse compression technique *Appl. Phys. Lett.* **68** 2793–5
[9] Kornelis W Helbing F Heinrich A, Couairon A Mysyrovicz A, Biegert J, Hauri C and Keller U 2004 Generation of intense, carrier-envelope phase-locked few-cycle laser pulses through filamentation *Appl. Phys.* B **79** 673
[10] Jarnac A *et al* 2014 Compression of tw class laser pulses in a planar hollow waveguide for applications in strong-field physics *Eur. Phys. J.* D **68** 373
[11] Russbueldt P *et al* 2015 Innoslab amplifiers *IEEE J. Sel. Top. Quantum Electron.* **21** 447–63
[12] Schulte J, Sartorius T, Weitenberg J, Vernaleken A and Russbueldt P 2016 Nonlinear pulse compression in a multi-pass cell *Opt. Lett.* **41** 4511
[13] Lavenu L, Natile M, Guichard F, Zaouter Y, Delen X, Hanna M, Mottay E and Georges P 2018 Nonlinear pulse compression based on a gas-filled multipass cell *Opt. Lett.* **43** 2252
[14] Grebing C, Mueller M, Buldt J, Stark H and Limpert J 2020 Kilowatt-average-power compression of millijoule pulses in a gas-filled multi-pass cell *Opt. Lett.* **45** 6250
[15] Russbueldt P, Weitenberg J, Schulte J, Meyer R, Meinhardt C, Hoffmann H D and Poprawe R 2019 Scalable 30 fs laser source with 530 w average power *Opt. Lett.* **44** 5222
[16] Kaumanns M, Pervak V, Kormin D, Leshchenko V, Kessel A, Ueffing M, Chen Y and Nubbemeyer T 2018 Multipass spectral broadening of 18 mJ pulses compressible from 1.3 to 41 fs *Opt. Lett.* **43** 5877–80
[17] Balla P *et al* 2020 Postcompression of picosecond pulses into the few-cycle regime *Opt. Lett.* **45** 2572
[18] Renchong Lv, Wang X, Teng H Zhu J Song J, Wang Z and Wei Z 2021 Generation of 172 fs pulse from a Nd: YVO_4 picosecond laser by using multi-pass-cell technique *Appl. Phys.* B **127** 50
[19] Fritsch K, Poetzlberger M, Pervak V, Brons J and Pronin O 2018 All-solid-state multipass spectral broadening to sub-20 fs *Opt. Lett.* **43** 4643–6
[20] Rueda P, Videla F, Witting T, Torchia G A and Furch F J 2021 8fs laser pulses from a compact gas-filled multi-pass cell *Opt. Express* **29** 27004
[21] Weitenberg J *et al* 2017 Multi-pass-cell-based nonlinear pulse compression to 115 fs at 7.5 μJ pulse energy and 300 w average power *Opt. Express* **25** 20502–10
[22] Nubbemeyer T Pervak V Kaumanns M, Kormin D and Karsch S 2021 Spectral broadening of 112 mJ, 13 ps pulses at 5 kHz in a LG10 multipass cell with compressibility to 37 fs *Opt. Lett.* **46** 929
[23] Khazanov E A, Mironov S Y and Mourou G A 2019 Nonlinear compression of high-power laser pulses: compression after compressor approach *Phys.-Usp.* **62** 1096–124
[24] Heyl C M *et al* 2016 Scale-invariant nonlinear optics in gases *Optica* **3** 75
[25] Klenke A, Kienel M, Eidam T, Hädrich S, Limpert J and Tünnermann A 2013 Divided-pulse nonlinear compression *Opt. Lett.* **38** 4593
[26] Guichard F, Zaouter Y, Hanna M, Morin F, Hönninger C, Mottay E, Druon Fedéric and Georges P 2013 Energy scaling of a nonlinear compression setup using passive coherent combining *Opt. Lett.* **38** 4437
[27] Herriott D R and Schulte H J 1965 Folded optical delay lines *Appl. Opt.* **4** 883
[28] Hanna M, Délen X, Lavenu L, Guichard F, Zaouter Y, Druon Fedéric and Georges P 2017 Nonlinear temporal compression in multipass cells: theory *J. Opt. Soc. Am.* B **34** 1340
[29] Engel G S and Moyer E J 2007 Precise multipass herriott cell design: Derivation of controlling design equations *Opt. Lett.* **32** 704
[30] Ueffing M, Reiger S, Kaumanns M, Pervak V, Trubetskov M, Nubbemeyer T and Krausz F 2018 Nonlinear pulse compression in a gas-filled multipass cell *Opt. Lett.* **43** 2070
[31] Arai K 2013 On the accumulated round-tripgouy phase shift for a generaloptical cavity *LIGO Scientic Collaboration* LIGO-T1300189-v1
[32] Seidel M, Balla P, Binhammer T, Frede M, Arisholm G, Winkelmann L, Hartl I and Heyl C M 2020 Hybridizing multi-pass and multi-plate bulk compression *EPJ Web Conf.* **243** 21001
[33] Hanna M, Daniault L, Guichard F, Daher N, Délen X, Lopez-Martens R and Georges P 2021 Nonlinear beam matching to gas-filled multipass cells *OSA Contin.* **4** 732
[34] Seidel M, Arisholm G, Brons J, Pervak V and Pronin O 2016 All solid-state spectral broadening: an average and peak power scalable method for compression of ultrashort pulses *Opt. Express* **24** 9412
[35] Südmeyer T, Marchese S V, Hashimoto S, Baer C R E, Gingras G, Witzel B and Keller U 2008 Femtosecond laser oscillators for high-field science *Nat. Photon.* **2** 599–604